Diagnosis of EGFR exon21 L858R point mutation as lung cancer biomarker by electrochemical nanoparticles modified pencil graphite electrode

Yalda Shoja, Ahmad Kermanpur, Fathallah Karimzadeh

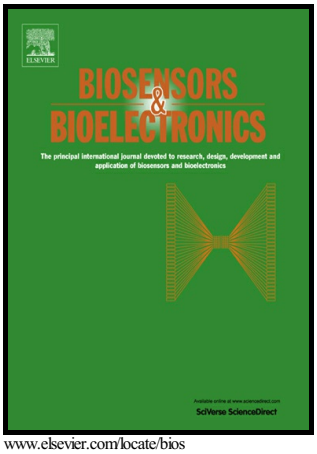

www.elsevier.com/locate/bios

PII: S0956-5663(18)30269-0
DOI: https://doi.org/10.1016/j.bios.2018.04.013
Reference: BIOS10409

To appear in: *Biosensors and Bioelectronic*

Received date: 10 January 2018
Revised date: 21 March 2018
Accepted date: 6 April 2018

Cite this article as: Yalda Shoja, Ahmad Kermanpur and Fathallah Karimzadeh, Diagnosis of EGFR exon21 L858R point mutation as lung cancer biomarker by electrochemical nanoparticles modified pencil graphite electrode, *Biosensors and Bioelectronic,* https://doi.org/10.1016/j.bios.2018.04.013

Diagnosis of EGFR exon21 L858R point mutation as lung cancer biomarker by electrochemical nanoparticles modified pencil graphite electrode

Yalda Shoja*, Ahmad Kermanpur, Fathallah Karimzadeh

Department of Materials Engineering, Isfahan University of Technology, Isfahan, P.O.Box 4156-83111, Iran.

y.shoja@ma.iut.ac.ir
yalda_shoja1981@yahoo.com

*To whom correspondence should be addressed. Fax: ++98-31 3391 2752

Abstract

In this present work we made a novel, fast, selective and sensitive electrochemical genobiosensor to detection of EGFR exon 21 point mutation based on two step electropolymerization of Ni(II)-oxytetracycline conducting metallopolymer nanoparticles (Ni-OTC NPs) on the surface of pencil graphite electrode (PGE) which was modified by reduced graphene oxide/carboxyl functionalized ordered mesoporous carbon (rGO/f-OMC) nanocomposite. ssDNA capture probe with amine groups at the5′ end which applied as recognition element was immobilized on the rGO/f-OMC/PGE surface via the strong amide bond. Ni-OTC metallopolymer NPs were electropolymerized to rGO/ssDNA-OMC/PGE surface and then hybridization fallows through the peak current change in differential pulse voltammetry (DPV) using Ni-OTC NPs as a redox label. The biosensor was characterized by field emission scanning electron microscopy (FE-SEM), X-ray diffraction (XRD), FT-IR spectroscopy, energy

dispersive X-ray spectroscopy (EDX), cyclic voltammetry and Nitrogen adsorption–desorption analysis. The Ni-OTC current response verified only the complementary sequence indicating a significant reduction current signal in comparison to single point mismatched and non-complementary and sequences. Under optimal conditions, the prepared biosensor showed long-term stability (21 days) with a wide linear range from 0.1 µM to 3 µM with high sensitivity (0.0188 mA/µM) and low detection limit (120 nM).

Graphical abstract

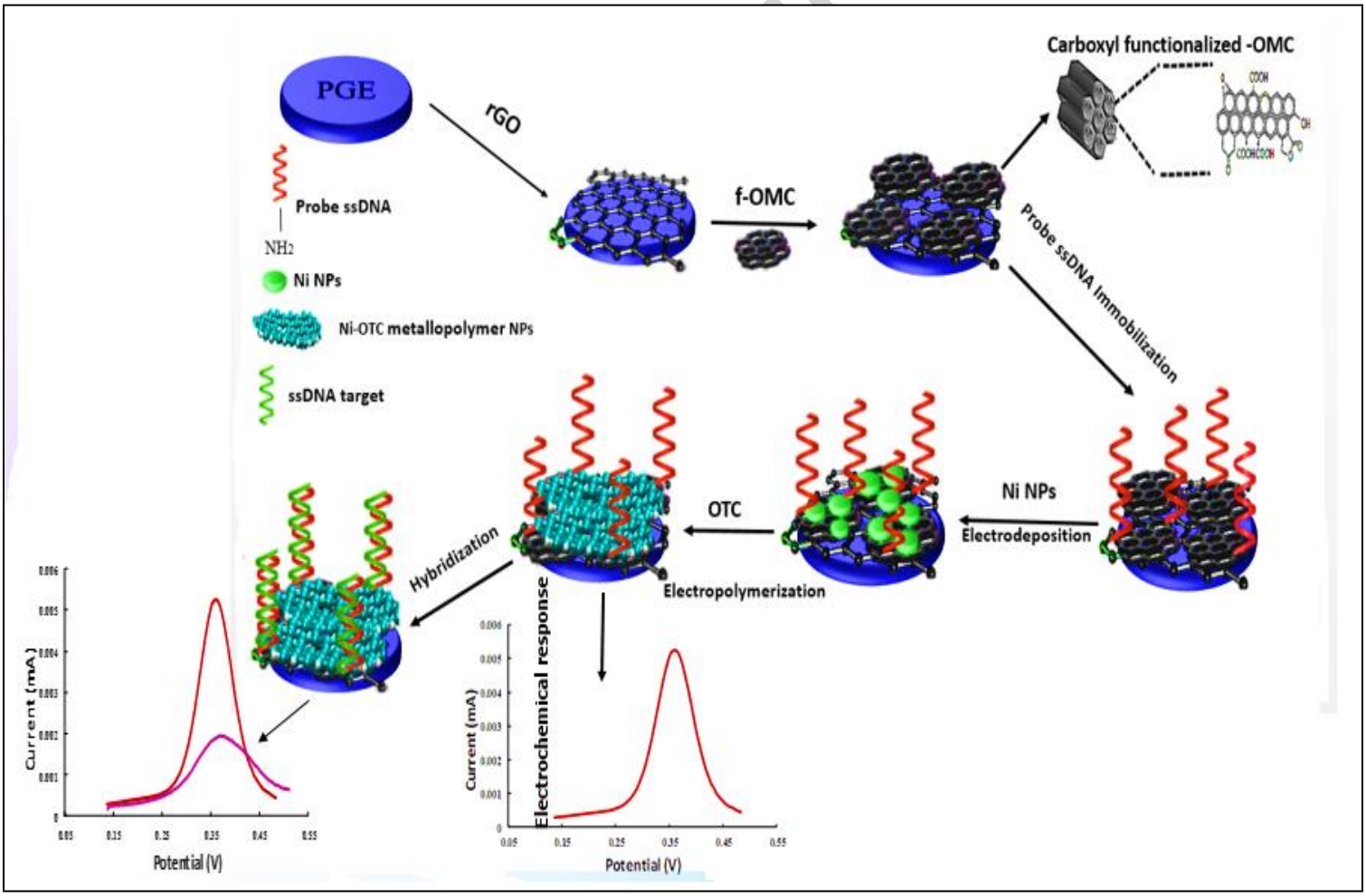

they can be genes or gene products, molecules, specific cells, hormones or enzymes and they can be assessed in various biological media such as urine, tissues, blood and sputum (Li et al., 2012; Kumar et al., 2006; Topkaya et al., 20162; Diamandis, 2010). In associated with their own specific application biomarkers are extremely significant in personalized medicine including diagnosis, prediction and management of targeted therapies (Ziegler et al., 2012).The quantitative and qualitative analysis of cancer biomarkers provide the basic information about the cell differentiation, the tumor on the tissue histogenesis, and cell functionalization which early detection of primary cancer, prognosis, cancer categorization and therapeutic guidelines can be possible through these basic information (Li et al., 2012; Finn, 2005; Wang et al., 2005). Changes to the DNA at the cellular level have seen in all type of cancers and these changes can be evaluated in the tumor tissue (Ziegler et al., 2012; Tian et al., 2017; Lin et al., 2013; Xu et al., 2016; Shtivelman et al., 2014). Non-small cell lung carcinoma (NSCLC) with epidermal growth factor receptor (EGFR) mutations is reported for more than 80% of all lung cancer cases with a poor prognosis. (Xu et al., 2016; Cancer Genome Atlas Research Network, 2012; Schiller et al., 2002; Wang et al., 2015; Hirsch and Bunn, 2009; Mok et al., 2009) .In fact, EGFR is a DNA tumor biomarker by which only the absence or presence of a mutation in a gene is determined (Ziegler et al., 2012; Xu et al., 2016).Two main usual EGFR gene mutations mostly occurred in exon 18–21, and exon19 which are a point mutation in exon 21 (L858R), and a 15-bp in-frame deletion in exon 19 (delE746-A750), respectively. These two mutations, which account for about 90% of cases with EGFR mutations, exhibit the most sensitivity to TKI that leads to enhancement of the activity of tyrosine kinase (Tian et al., 2017; Takata et al., 2015; Mitsudomi and Yatabe, 2007). Therefore, it can be said that accurate sensing of EGFR as a cancer

biomarker is of main clinical importance for diagnosis and treatment approaches in NSCLC (Brenner and Normolle, 2007; Frank and Hargreaves, 2003).

Recently, various techniques have been reported for the detection of cancer biomarkers including fluorescence immunoassay (Yong et al., 2009; Wu et al., 2002), spectrophotometric or optical methods (Wang et al., 2009a), radioimmunoassay (Chan et al., 1997), electrochemical analysis (Prabhulkar et al., 2009; Barton et al., 2008; Tang et al., 2008), capillary electrophoresis and chromatographic analysis (Yang et al., 2010). Generally optical methods are useful and reliable for the sensing of many types of disease biomarkers with multiple signals (Vellaisamy et al., 2018; Wang et al., 2016; Ma et al., 2017; Ying et al., 2017) but among all these methods, electrochemical approaches are considerably suitable ones, because of their unique features like fast response, portability, facility, great sensitivity, wide range of detection limit and inexpensive cost. The assay of cancer biomarkers have been carried out by electrochemical biosensors as an advantageous analytical method (Tian et al., 2017; Xu et al., 2016; Wang, 2006a; Chikkaveeraiah et al., 2012). However, wide range cancer biomarkers examination requires the improvement of highly accurate and sensitive, and fast responding traditional electrochemical DNA cancer biomarker biosensors (Wang, 2006a). Therefore, associating of electrochemical biosensors with nanomaterial, such as variety of metal nanoparticles (NPs), reduced graphene oxide (rGO) and other nanostructured materials offers amplified sensitivity for identification of cancer biomarkers (Farzin and Shamsipur, 2018; Wang, 2007). In this consideration, ordered mesoporous carbon (OMC), as a novel carbon nanostructure material, has been widely interested due to their special properties including chemical and thermal stabilities, high specific surface area, uniform structural and large pore volume (Luo et al., 2013; Wang et al., 2009b; Joo et al., 2001). Moreover, investigation proved well-ordered pore structure of OMC make it appropriate

support to load metal and metallic complex NPs including conducting metallopolymers NPs as an efficient nanocomposite (Kang et al., 2010; Kazemi and Mohamadi, 2013). Also, the functionalization or modification of OMC providing the active sites on its surface for chemical immobilization of DNA and proteins (Vinu et al., 2007). Recently rGO has attracted many attentions duo to its divers uses in wide ranging from electrode materials to electronic devices for sensors, fuel cells and transistors because of its distinguished properties, such as large surface area, extraordinary electron transport rate, excellent electrical and thermal conductivity, tunable band gap and great mechanical strength. (Song et al., 2016; Zhang et al., 2010; Tan and lee, 2013).

The pencil graphite electrode (PGE) is an important electrode material which can be used in construction of every type electrochemical biosensors due to its advantages such as single-use disposable electrode, low cost, low background current and commercial availability (Ozcan and Sahin, 2010; Rezaei et al., 2015; Rana and Kawde, 2016).

In this study, we have synthesized a nanocomposite consisting of rGO, OMC and Ni-oxytetracycline (Ni-OTC) conducting metallopolymer NPs as an electroactive label, to fabricate the electrochemical biomarker biosensor. To the best of our knowledge, the utilization of such nanocomposite for electrochemical identification point mutation, L858R, of EGFR exon 21 has not been reported. Herein, single-stranded DNA (ssDNA) was immobilized on PGE modified by rGO/f-OMC through chemical immobilization. In the next step, Ni NPs were electrodeposited on DNA-modified PGE and finally OTC was electropolymerized on Ni NPs as metal source to obtain rGO/f-OMC-DNA/Ni-OTC NPs/PGE. Finally the developed biosensor was characterized by FE-SEM, EDS, FT-IR and CV techniques.

2. Experimental

2.1. Chemicals and apparatus

rGO was prepared from Neutrino Co. (Iran). Tetraethyl orthosilicate (TEOS), sucrose, hexadecyltrimethylammonium bromide (CTAB), was from Merck. OTC raw material was from DarouPakhsh Co. (Iran). Sodium hydroxide, Nickel (II) sulfate, sulfuric acid, *N*-hydroxysulfosuccinimide (NHS) and 1-Ethyl-3-(3-dimethylaminopropyl) carbodiimide (EDC) were prepared from Sigma–Aldrich. All the other chemicals were of analytical grade. All the solutions were prepared with deionized water and deoxygenated by highly pure nitrogen gas for at least 10 min before experiments. All oligonucleotides were synthesized and purified by Takapouzist Co. (Tehran, Iran). Single-stranded DNA capture probe (ssDNA), which is as a bioreceptor for exon 21 point mutation (L858R), was an amine terminated 15- bases sequence: NH_2- 5' TTT GGC CCG CCC AAA3' . The sequence of 15-bases perfectly complementary target ssDNA ($ssDNA_c$) for ssDNA capture probe was shown as: 5' TTT GGG CGG GCC AAA3' . The sequence of 15-bases DNA target with a point mutation $ssDNA_M$, (a T-G mismatch that indicated by the underline) for ssDNA probe was as fallow: 5' TTT GGG CTG GCC AAA3') and the non-complementary DNA oligonucleotide sequence ($ssDNA_{NC}$), was 5' CAT ATT TGC CAA CAG3' . Stock solutions stored at 4 °C until use.

Electrochemical measurements were performed with AMETEK advanced electrochemical system (model: PARSTAT 2273), driven with Electrochemistry PowerSuite Software. A conventional electrochemical 3 electrode system was used for all electrochemical experiments with an Ag/AgCl electrode (saturated potassium chloride), a PGE (diameter 1 mm) and a platinum wire as reference, work and counter electrodes respectively. The pencil lead electrode was fabricated from a .typical HB#2 pencil (Brand name Staedtler, Germany).

X-ray diffraction analysis was obtained using a Philips X'Pert-MP instrument and the patterns were measured using Cu-Kα radiation. Structural and EDS analyses were conducted using a scanning electron microscope (VEGA TESCAN SEM). FT-IR spectroscopic analysis was performed by a FT-IR spectrophotometer (Jasco 680-plus, Tokyo, Japan) in the range of 7000–400 cm^{-1} using KBr powder-pressed pills. The ultrasonic water bath (LBS2‑FALC) with time and temperature control was used for the dispersion of nanomaterials. Nitrogen adsorption–desorption isotherms were measured at 77 º K by a BELSORP MINI II instrument (BEL, Japan).

All electroanalytical measurements were carried out at room temperature and in air pressure.

2.2. Synthesis of carboxylic functionalized OMC (f-OMC)

Mesoporous silica named MCM-41 and sucrose were selected as a template and the carbon source respectively for OMC preparation. Mesoporous silica MCM-41 was synthesized according to the procedure described by Cai et al. (2001). Then OMC was prepared according to the previously reported procedure (Lin et al., 2006).The resultant carbon–silica composite was boiled after pyrolysis in 1 M NaOH solution dissolved in 50:50 mixture of ethanol and water for 1 h to remove the silica framework. Then the template-free carbon product was filtered, washed with water, and dried at 100 °C (Kim et al., 2004). Afterwards, the OMC was functionalized with carboxylic groups through acid treatment to obtain modified surface. For this purpose, the OMC was modified with concentrated H_2SO_4 for 3 h at 80 °C according to the procedure in literature (Dong et al., 2010; Zhu et al., 2005).

2.3 Preparation of rGO/f-OMC/PGE

Faber-Castell HB#2 pencil was chosen as working electrode and the wood coverage from the top 2 cm of the pencil was cut using a small teeth saw until the pencil lead was fully exposed and

easily can be attached to crocodile clips. Then the other side of graphite pencil was polished and smoothed with 150-grit sandpaper, before being treated. Afterward, the polished PGE surface was pretreated in 0.8M NaOH solution by scanning the potential between 1.3 and 1.9 V with a scan rate of 100 mV s^{-1} for 50 cycle (Rana and Kawde, 2016). Then 10 mg of rGO nanosheet was dispersed in 10 mL of acetone by ultrasonicated bath for 30min. The PGE modified with rGO nanosheet by dropping the 20 µL of rGO/acetone suspension on the PGE surface by micropipette and the PG electrode was dried at room temperature. Thereafter the synthesized f-OMC (10 mg) was dispersed in 10 mL N,N-dimethyl formamide (DMF) and the suspension was sonicated for 30 min to obtain a homogeneous black mixture. Then 20 µL of the prepared suspension was dropped on the PGE surface and was dried at room temperature (Kerman et al., 2002). In this way the rGO/f-OMC/PGE was obtained.

2.4 Fabrication of rGO/ssDNA-OMC/Ni-OTC NPs biosensor

For immobilization of amine-terminate ss DNA capture probe, firstly the carboxyl group of rGO/f-OMC/PGE must be activated. Therefore, the rGO/f-OMC/PGE was immersed in 50 mM phosphate buffer solution (pH 7.40) containing 5mM NHS and 2mM EDC for 60 min. The obtained rGO/OMC-linker/PGE was rinsed with the 50mM phosphate buffer solution (pH 7.40) at room temperature and then it was inverted. Subsequently10 µL ssDNA capture probe (5 µM) was dropped onto the rGO/OMC-linker/PGE surface and amine-terminate ssDNA is covalently immobilized to the electrode surface via an amide bond and the rGO/ssDNA-OMC/PGE was constructed. At the end the modified electrode was washed by phosphate buffer solution to remove unbound ssDNA and it was dried at air overnight (Kerman et al., 2002). In the next step, to prepare the rGO/ssDNA-OMC/Ni-OTC NPs/PGE, two step electrochemical technique was

used for electrodeposition of conducting metallopolymer of Ni-OTC NPs on rGO/ssDNA-OMC/PGE (Vinu et al., 2007). For this purpose, firstly an aqueous solution of 1 M H_2SO_4 solution containing 0.2 M $NiSO_4$ was used for electrodeposition of Ni NPs by applying constant potential at −1.25 V for 300 s (Guo et al., 2015). Finally, electropolymerization of Ni-OTC was carried out by using successive cyclic voltammetry of the rGO/ssDNA-OMC/Ni-NPs/PGE in an alkaline solution of 1×10^{-4} mM of OTC between 0.1 and 0.9 V at scan rate 50 mV s^{-1} for at least 15 cycles. All the fabrication steps of described before are shown in Scheme 1.

2.5. Hybridization with complementary target ssDNA

$ssDNA_c$ target hybridization that is joining two complementary strands of DNA to form a double-stranded molecule, with the ssDNA capture probe immobilized on the PGE modified surface was considered by immersing rGO/ssDNA-OMC/Ni-OTC NPs/PGE in 100 µL of 50 mM phosphate buffer solution (pH 7.0) containing different concentrations of ssDNA target for 60 min at 37 °C. The investigation of one-base mismatch ssDNA interactions was also studied by incubated the modified PGE in 100 µL of 50 mM phosphate buffer solution (pH 7.0) containing specified amount of one-base mismatch ssDNA. Finally, the obtained PG electrode should be rinsed with the PBS buffer and doubly distilled water to remove unhybridized ssDNA targets.

2.6 Electrochemical detection

Cyclic voltammetry was used as an effective technique for characterization of developed ssDNA biosensor in 1.0mM $K_3Fe(CN)_6/K_4Fe(CN)_6$ (1:1) mixture containing 0.1 M KCl. Differential pulse voltammetry (DPV) and amperometry techniques were applied for the

detection of hybridization via the change in electrochemical response of Ni-OTC NPs as electrochemical active label. The DPV parameters were adjusted as follows: pulse amplitude 25 mV, pulse width 50 ms and scan rate 10 mVs^{-1}.

3. Results and discussion

3.1 Characteristics of rGO/ssDNA-OMC/Ni-OTC NPs modified electrode

The crystalline structure of the MCM-41 silica particles was deduced from the XRD pattern, as shown in Fig. S1a. Two Bragg peaks which can be indexed as (100) and (110) are related to MCM-41 (Cai et al., 2001). Fig. S1b demonstrates the XRD pattern of the OMC and the existence of low-angle peak confirming the crystalline mesoporous carbon synthesized from MCM-41 (Lin et al., 2006). Morphology of the prepared OMC deposited on rGO/PGE surface was characterized using FE-SEM images as shown in Fig. S1c. As can be seen, porous carbon particles kept the crystal and isolated segment morphologies after removal of the MCM-41 as template and they are well dispersed on rGO/PGE surface (Li et al., 2014). N_2 adsorption–desorption isotherms for prepared OMC are demonstrated in Fig. S1d. After removal of silica template, prepared OMC exhibits a type IV isotherm with a sharp capillary condensation steps which imply to uniformity and ordered of mesoporous network. Also for the prepared OMC the capillary condensation step happens at a relative pressure of about 0.4, which is in accordance with other similar works which were previously reported (Gierszal et al., 2008). This results indicate as-synthesized OMC shows porosity with a narrow size distribution. The pore size distribution was calculated by BJH method using adsorption brunch (Fig. S1d, inset). According to BJH results, pores major size of prepared OMC was appeared 4.1 nm in diameter. Finally

specific surface area of prepared OMC was calculated about 926.56 m^2/g using the BET method and total pore volume was 1.31 cm^3/g (Die et al., 2010).

XRD pattern of the Ni nanoparticles is demonstrated at Figs. 1a. Diffraction peaks at about 45º (111), 52º (200), 78º (220) and 94º (311) are corresponding to face centered cubic crystal structure (fcc) of Ni NPs without any noticeable traces of any impurity which electrodeposited on rGO/f-OMC/PGE (Gopalan et al., 2010). These diffraction peaks are in agreement with the Joint Committee on Powder Diffraction Standards cards (JCPDS) nos. 04-0850.

Fig. 1b is FE-SEM image of the modified rGO/OMC/PGE surface after Ni NPs electrodeposition. As can be seen in this figure, electrodeposited Ni NPs on the rGO/OMC/PGE surface have a uniform and condensed distribution in the range 25-50 nm in diameter. The electrodeposition of Ni NPs was accompanied with the formation and growth of bubbles on the work electrode surface that it may be related to simultaneous hydrogen reduction. It can be said this process affects on diffusion and reaction mechanism of Ni^{2+} ions on electrode surface and leads to compacted morphology and distribution of Ni nanoparticles (Guo et al., 2015).

The FT-IR spectra of f-OMC (curve a) and ssDNA-OMC (curve b) are represented in Fig. S2. A strong peak about at 1730 cm^{-1} in FT-IR spectrum, (curve a), is assigned to the carboxyl group stretching vibration of f-OMC. The bands emerged at about 1669 cm^{-1} in curve b due to the presence of amide II which is indicated amine-terminate ssDNA capture probe covalently attached to f-OMC (Shoja et al., 2016a). The region from 818 cm^{-1} to 1285 cm^{-1} is attributed to stretching vibrations of DNA phosphate groups (Ede et al., 2015). Vibration bands of N-H, C-H and C=O stretching in the DNA bases were appeared at the 1547, 2934 and 1743 cm^{-1} respectively (Radhakrishnan et al., 2013). These vibration frequencies prove the chemical immobilization of ssDNA on rGO/f-OMC nanocomposite.

Electrochemical polymerization of OTC ligand was carried out by applying consecutive cyclic potential scan technique in the absence of dissolved Ni ions in alkaline solution of OTC which leads to the formation of isolated Ni-OTC NPs. on rGO/ssDNA-OMC/Ni NPs/PGE. Successive cyclic voltammograms of the rGO/ssDNA-OMC/Ni NPs/PGE in 0.5 M NaOH solution containing 1×10^{-4} M of OTC are presented in Fig. 3Sa which displays progressive increase in Faradaic peak current intensities about 0.4 V vs. Ag/AgCl with every scanned cycle in this voltammograms. This process is corresponded to Ni (II/III) redox reaction in the polymer texture (Kazemi and Mohamadi, 2013). Increasing in anodic and cathodic peak currents continued gradually with increasing scan number for up to 18 cycles and then the peak current remained stable. Therefor the 18 cycles were selected as the applied number of electropolymerization cycles.

The chemical structure of OTC and the very possibly structure of the Ni‑OTC complex are illustrated in Fig. 2a. OTC has a special conjugated structure including an amid group and α,β unsaturated ketone form. It can be said that conductivity of the Ni-OTC NPs results from possible overlapping between Ni orbitals and OTC conjugated structure (Kazemi and Mohamadi, 2013; Amin et al., 2017). Fig. 2b depicts the structure and morphology of Ni-OTC NPs using FE-SEM image. As it is clear, Fig. 2b verified formation of Ni-OTC uniform nanostructure film that consisted of Ni-OTC NPs, with average size about 58-95 nm, by electropolymerization of OTC ligand in the absence of dissolved Ni ions in NaOH solution. The EDS spectrum revealed that the surface of rGO/ssDNA-OMC/Ni-OTC NPs/PGE contained C, N, O, P and Ni elements with 36.66, 6.42, 33.99, 10.14 and 12.79 wt. %, respectively (Fig. S3b). The existence of P is individually related to ssDNA probe.

3.2. Electrochemical behavior of the modified electrodes

Cyclic voltammetry is an efficient technique for electrochemical investigation of developed DNA biosensor. In this regard, electron transfer rate and reversibility are two significant electrochemical parameters that are related to the peak height and separation, respectively. Investigating of peak height and separation were done by studying cyclic voltammograms of different modified electrodes in 0.1 M KCl solution, containing 5.0 mM $K_3[Fe(CN)_6]$ at scan rate of 100 mVs^{-1}. The results showed that peaks current intensity and potential peak separations for $[Fe\ (CN)_6]^{3-}/[Fe\ (CN)_6]^{4-}$ redox at rGO/f-OMC/PGE (curve b) were higher and smaller than PGE (curve a), respectively, indicating faster electron transfer rate and more reversibility for modified rGO/f-OMC/PGE (Fig. 3). Moreover, this remarkable response toward $[Fe\ (CN)_6]^{3-}/[Fe\ (CN)_6]^{4-}$ redox at rGO/f-OMC/PGE surface may be corresponded to increasing mass transfer and accelerating the electron transfer rate caused by large pore volume, large effective surface area, proper electrically conductive and large density of carboxyl group or edge plane sites of rGO/f-OMC surface nanocomposite (Luo et al., 2012). When Ni-OTC NPs were formed on rGO/f-OMC/PGE, redox peak current and reversibility for $[Fe\ (CN)_6]^{3-}/[Fe\ (CN)_6]^{4-}$ reaction considerably increased (curve c). It can be concluded that Ni-OTC NPs have an electrocatalytic effect, preparing more active sites for the electrooxidation of $[Fe\ (CN)_6]^{3-}/[Fe\ (CN)_6]^{4-}$. Also the well-defined anodic and cathodic peaks appeared at about 0.66 and 0.51 V (curve c) are due to redox reaction of the Ni(III)/Ni(II) couple at the rGO/f-OMC/Ni-OTC NPs/PG electrode surface (Shoja et al., 2016b). After immobilization of ssDNA capture probe on the modified PGE, the rGO/ssDNA-OMC/Ni-OTC NPs/PGE (curve d) exhibited less reversibility than the other modified electrodes (curve b, c) which was related to the electrostatic repulsion between the negatively charged ss DNA capture probe and $[Fe\ (CN)_6]^{3-}/[Fe\ (CN)_6]^{4-}$.

Furthermore the redox peak of Ni (III)/Ni (II) was not observed at rGO/ssDNA-OMC/Ni-OTC NPs/PGE. It can be due to the interaction between Ni-OTC NPs and ssDNA capture probe which causes the shielding of the Ni (III)/Ni (II) redox peak. Also this result confirms ssDNA capture probe immobilized on modified PGE by rGO/f-OMC nanocomposite. For more electrochemical investigation, cyclic voltammograms of rGO/f-OMC/Ni-OTC NPs/PGE and rGO/ssDNA-OMC/Ni-OTC NPs/PGE were obtained at scan rates ranging from 10 to 100 mV/s in 5.0 mM $K_3[Fe(CN)_6]$ solution which are shown in Fig. S4a and Fig. S4b, respectively. Anodic peak currents were increased in a linear relationship with the square root of scan rates for both electrodes (Fig. 4). This illustrates that the process of $[Fe(CN)_6]^{3-}/[Fe(CN)_6]^{4-}$ redox is mainly diffusion controlled at the surface of both rGO/f-OMC/Ni-OTC NPs/PGE and rGO/ssDNA-OMC/Ni-OTC NPs/PGE.

3.3. Hybridization, selectivity and detection of L858R mutation

Hybridization of ssDNA capture probe with $ssDNA_c$ was monitored using DPV technique by applying rGO/f-OMC/Ni-OTC NPs/PGE as working electrode in which Ni-OTC NPs are as electroactive label. Fig. 5a presents DPV voltammograms of different rGO/f-OMC/Ni-OTC NPs/PGE, without ssDNA capture probe (curve a) and with (curve b), after hybridization with $ssDNA_c$ (curve c) and after hybridization with, $ssDNA_M$ (curve d) in NaOH (0.1 M). As is shown in Fig. 5b, rGO/f-OMC/Ni-OTC NPs/PGE displayed considerable response relating to the electrocatalytic activity of Ni-OTC NPs as redox label. By immobilization of ssDNA capture probe, rGO/ssDNA-OMC/Ni-OTC NPs/PGE, the electrochemical signal of Ni-OTC NPs was decreased owing to probable interaction between Ni-OTC NPs and free DNA bases. After hybridization with complementary target, electrochemical response of biosensor diminished

significantly due to strong interaction of Ni-OTC NPs with base pairs in helix DNA. In order to more investigate the selectivity of prepared DNA biosensor, responsibility of biosensor studied at presence of other highly potential interferences such as $ssDNA_{NC}$ and duplex DNA. According to the results influence of $ssDNA_{NC}$ and duplex DNA on the developed DNA biosensor response to detection of $ssDNA_c$ was very negligible.

According to these results the most probable mechanism for redox process of electrode modified by Ni-OTC NPs can be expressed as follows:

$$[\text{Ni(II)-OTC}] + OH^- \longrightarrow [\text{Ni(II)-OTC (OH)}]^- \quad (1)$$

$$[\text{Ni (II)(OH)-OTC}]^- + 2OH^- \longrightarrow [\text{Ni(III)(O)(OH)-OTC}]^{2-} + H_2O + e^- \quad (2)$$

It is clearly electrostatic repulsion between the negatively charged hydroxyl ions (OH^-) and both of ssDNA capture probe and helix DNA, disrupted the redox process of Ni-OTC NPs. Therefore in the presence of ssDNA and helix DNA intensity current of Ni-OTC redox decreased.

At the end, control experiment was done via expose of rGO/ssDNA-OMC/Ni-OTC NPs/PGE to the one-base mismatch oligonucleotide. The results illustrated the remarkable response of Ni-OTC metallopolymer NPs was gained from rGO/f-OMC/Ni-OTC NPs/PGE and the weakest signal was corresponded to full hybridization of rGO/ssDNA-OMC/Ni-OTC NPs/PGE with $ssDNA_c$.

3.4. Optimization of hybridization condition for analytical application

It is clear that immobilized ssDNA capture probe surface concentration and hybridization time can affect the biosensor performance. Both of these parameters were optimized by following current changes of modified electrode in NaOH 0.1 M using DPV technique. At first,

optimum surface concentration of ssDNA capture probe was obtained by detection of minimum anodic current of rGO/ssDNA-OMC/Ni-OTC NPs/PGE at different concentration of immobilized ssDNA capture probe and specific $ssDNA_c$ concentration (5 µM). As can be seen from Fig. S5a, electrochemical response of the work electrode decreased with increasing ssDNA capture probe concentration from 0.5 µM to 5 µM and then increased as the ssDNA capture probe concentration went higher than 5 µM. This result is mostly due to the steric effect and repulsive electrostatic that increase with enhancement ssDNA capture probe concentration (Peterson et al., 2001). Afterward owing of determination optimum time hybridization and its influence on biosensor response, anodic peak current of biosensor was investigated for rGO/ssDNA-OMC/Ni-OTC NPs/PGE at 5 µM of immobilized ssDNA capture probe and defined $ssDNA_c$ (5 µM) at different hybridization time (Fig. S5b). The results showed most hybridization reaction happened at 60 min because the response of biosensor decreased as the time hybridization increased from 15 min to 60 min and then it stayed approximately unchanged. Therefor 5 µM and 60 min choose as optimal condition for hybridization and subsequent experiments were done under the optimum condition at 37 ºC.

3.5. Sensitivity and calibration curve at different concentrations of ssDNA target

Chronoamperometry technique was applied for examining sensitivity of the developed DNA biosensor in this study. The chronoamperograms obtained by measurement modified biosensor response at different concentrations of complementary $ssDNA_c$ in the range of 0.1 µM to 3 µM under optimized condition. As expected, with increasing concentration of $ssDNA_c$, the measured current at 0.2 s is decreased and then for each chronoamperometry curve, output current decays with time according to Cottrell equation (Fig. 6) (Choudhary et al., 2015; Wang,

2006b). Fig. S6 shows the respective calibration curve of rGO/ssDNA-OMC/Ni-OTC NPs/PGE with correlation coefficients of 0.998 (for n=9). Linear regression equation between peak current and the $ssDNA_c$ concentration was obtained as; I (mA) = ─0.0188x C (µM) + 0.0577 mA and using three times the standard deviation of the blank (background) signal, detection limit was calculated 120 nM. Table 1 shows a comparison between performances of some previously reported electrochemical DNA biosensor and our modified DNA biosensor in this work. A wide linear range, the good linear response to the ssDNA target concentration (R^2= 0.998) and very high sensitivity (0.0188 mA/µM) of proposed electrochemical DNA biosensor in this study can be comparable previously reported works. Therefore, it can be said, the prepared DNA biosensor possessed an excellent sensitivity that results from synergistic effect between rGO sheets and f-OMC which provides not only high effective surface area for the immobilization of Ni-OTC nanostructure metallopolymer but also active sites for ssDNA chemical immobilization. Moreover, compared to other DNA biosensors in which metal complexes are used as an electroactive label for monitoring of DNA hybridization (Noorbakhsha and Salimi, 2011; Miodek et al., 2016), the usage of Ni-OTC NPs in construction of biosensors as an electroactive label is very simple, low cost and efficient method via electrochemical deposition and there is no need for complicated synthesis steps.

3.6. Stability and repeatability of electrochemical biosensor

The stability of electrochemical DNA biosensor was measured by evaluation of the biosensor response for a period of 3 weeks under its storage at 4 °C in PBS 50 mM (pH = 7.0). The developed DNA biosensor retains 70% of maximum initial current response at the first day of fabrication after 2 weeks and finally the current response of

the biosensor decreased to 65% of its original response after 3 weeks. This shows that the present DNA biosensor has good stability. Furthermore, this DNA biosensor shows approximately the same response after 5 successive hybridization in a constant concentration of target DNA (5 µM) and relative standard deviations (RSD) was calculated 3.7% indicating good repeatability for the produced biosensor in this work.

4. Conclusion

In summary, a sensitive electrochemical DNA biosensor based on rGO/f-OMC/Ni-OTC NPs/PGE for identification point mutation, L858R, of EGFR exon 21 was successfully constructed. rGO and f-OMC were deposited onto electrode surface respectively to improve electrical conductivity and electrochemical effective surface area. Amine functionalized ssDNA capture probe immobilized on PGE was modified by rGO/f-OMC/PGE via amid bond formation and then Ni-OTC metallopolymer NPs were formed on rGO/ssDNA-OMC/PGE as redox label in two step electrochemical procedure. Under the optimized condition, the present electrochemical DNA biosensor showed excellent sensitivity to hybridization of ssDNA target (0.0188 mA/µM) with good linear response (R^2 = 0.998) in wide concentration range and low detection limit (120 nM). This DNA biosensor possessed an inexpensive fabrication method, satisfactory stability and reproducibility. Modified rGO/f-OMC/Ni-OTC NPs/PGE is only suitable for the application in alkaline solution but it has potential utilization in the fabrication of other electrochemical DNA biosensor and even electrochemical immunosensor.

Acknowledgments

The authors greatly acknowledge the Iran National Science Foundation (INSF) and Isfahan University of Technology (IUT) Research Council for their support. The authors would like to thank Dr. J. Ghodsi and H.R. Abak for their useful comment.

References

Amin, R.R., Abo-Elkassem, M., Anwar, A., 2017. Res. Rev. J. Pharm. Pharm. Sci. 6, 38-48.

Atkinson, A.J., Colburn, W.A., DeGruttola, V.G., DeMets, D.L., Downing, G.J., Hoth, D.F., Oates, J.A., Peck, C.C., Schooley, R.T., Spilker, B.A., Woodcock, J., Zeger, S.L., 2001. Clin. Pharmacol. Ther. 69, 89-95.

Brenner, D.E., Normolle, D.P., 2007. Cancer Epidemiol. Biomark. Prev. 16, 1918-1920.

Barton, A.C., Davis, F., Higson, S.P.J., 2008. Anal. Chem. 16, 9411-9416.

Cai, Q., Luo, Z.S., Pang, W.Q., Fan, Y.W., Chen, X.H., Cui, F.Z., 2001. Chem. Mater. 304, 258-263.

Chan, D.W., Beveridge, R.A., Muss, H., Fritsche, H.A., Hortobagyi, G., Theriault, R., Kiang, D., Kennedy, B.J., Evelegh, M., Clin. J., 1997. J. Clin. Oncol. 15, 2322-2328.

Chen, M., Hou, C., Huo, D., Bao, J., Fa, H., Shen, C., 2016. Biosens. Bioelectron. 85, 684-691.

Cancer Genome Atlas Research Network, 2012. Nature 489, 519-525.

Chikkaveeraiah, B.V., Bhirde, A.A., Morgan, N.Y., Eden, H.S., Chen, X.Y., 2012. ACS Nano. 6, 6546-6561.

Choudhary, T., Rajamanickam, G.P., Dendukuri, D., 2015. Lab Chip. 15, 2064-2072.

Dai, W., Zheng, M., Zhao, Y., Liao, S., Ji, G., Cao, J., 2010. Nanoscale Res. Lett. 5, 103-107.

Diamandis, E.P., 2010. J. Natl. Cancer Inst.102, 1462‑1467.

Dong, J., Hu, Y., Zhu, S., Xu, J., Xu, Y., 2010. Anal. Bioanal. Chem. 396, 1755-1762.

Ede, S.R., Anantharaj, S., Nithiyanantham U., Kundu, S., 2015. Phys.Chem.Chem.Phys. 17, 5474-5484.

Finn, O.J., 2005. N. Engl. J. Med. 353, 1288-1290.

Farzin, L., Shamsipur, M., 2018. J. Pharm. Biomed. Anal. 147, 185-210.

Frank, R., Hargreaves, R., 2003. Nat. Rev. Drug Discov. 2, 566-580.

Gierszal, K.P., Jaroniec, M., Kim, T.W., Kim, J., Ryoo, R., 2008. New J. Chem. 32, 981-993.

Gopalan, V.E., Malini, K., Santhoshkumar, G., Narayanan, T., Al-Omari Ia, J.P., Kumar, D.S., Yoshida, Y., Anantharaman, M., 2010. Nanoscale Res. Lett. 5, 889-897.

Guo, H., Huang, Z., Zheng, Y., Weng, S., 2015. Int. J. Electrochem. Sci. 10, 10703-10712.

Hirsch, FR.; Bunn PA, Jr.; 2009. Lancet. Oncol. 10, 432-433.

Joo, S.H., Choi, S.J., Oh, I., Kwak, J., Liu, Z., Terasaki, O., Ryoo, R., 2001. Nature 412, 169‑172.

Kang, L., Wang, R.T., Kong, L.B., Li, H., Zhang, J., Luo, Y.C., 2010. Mater. Lett. 64, 2064-2067.

Kazemi, S.H., Mohamadi, R., 2013. Electrochim. Acta 109, 823‑827.

Kerman, K., Ozkan, D., Kara, P., Meric, B., Gooding, J.J., Ozsoz, M., 2002. Anal. Chim. Acta 462, 39-47.

Kim, J., Lee, J., Hyeon, T., 2004. Carbon 42, 2711-2719.

Kumar, S., Mohan, A., Guleria, R., 2006. Biomarkers. 11, 385-405.

Li, J., Li, S., Yang, C.F., 2012. Electroanalysis 24, 2213-2229.

Li, X., Zhou, J., wang, J., Qiao, W., Ling, L., Long, D., 2014. RSC Adv. 4, 62662-62665.

Lin, H.C., Zhang, F.L., Geng, Q., Yu, T., Cui, Y.Q., Liu, X.H., 2013. J. Proteome Res. 12, 3423-3433.

Lin, C.F., Zhang, X., Lin, H., Wang, N., Li, J.B., Yang, X.Z., 2006. Adv. Mater. Res. 11-12, 543-546.

Luo, L., Li, F., Zhu, L., Ding, Y., Zhang, Z., Deng, D., Lu, B., 2013. Colloids. Surf. B 102, 307-311.

Luo, L., Li, F., Zhu, L., Zhang, Z., Ding, Y., Deng, D., 2012. Electrochim. Acta 77, 179‑183.

Ma, W., Fu, P., Sun, M., Xu, L., Kuang, H., Xu, C., 2017. J. Am. Chem. Soc. 139, 11752-11759.

Mok, T.S., Wu, Y.L., Thongprasert, S.;Yang, CH.; Chu, D.T., Saijo, N., Sunpaweravong, P., Han, B., Margono, B., Ichinose, Y., Nishiwaki, Y., Ohe, Y., Yang, J.J., Chewaskulyong, B., Jiang, H., Duffield, E.L., Watkins, C.L., Armour, A.A., Fukuoka, M., 2009. N. Engl. J. Med. 361, 947-957.

Miodek, A., Omrani, N.M., Khoder, R., Youssoufi, H.K., 2016. Biosens. Bioelectron. 154, 446-454.

Mitsudomi, T., Yatabe, Y., 2007. Cancer Sci. 98, 1817-1824.

Noorbakhsh, A., Salimi, A., 2011. Biosens. Bioelectron. 30, 188‑196.

Ozcan, A., Sahin, Y., 2010. Biosens. Bioelectron. 25, 2497-2502.

Prabhulkar, S., Alwarappan, S., Liu, G.D., Li, C.Z., 2009. Biosens. Bioelectron. 24, 3524-3530.

Peterson, A.W., Heaton, R.J., Georgiadis, R.M., 2001. Nucleic Acids Res. 29, 5163-5168.

Rana, A., Kawde, A.N., 2016. J. Chin. Chem. Soc. 63, 668-676.

Rezaei, B., Boroujeni, M.K., Ensafi, A.A., 2015. Biosens. Bioelectron. 66, 490-496.

Radhakrishnan, S., Sumathi, C., Dharuman, V., Wilson, J., 2013. Anal. Methods. 5, 684-689.

Saberi, R.S., Shahrokhian, S., Marrazza, G., 2013. Electroanalysis 25, 1373-1380.

Schiller, J.H., Harrington, D., Belani, C.P., Langer, C., Sandler, A., Krook, J., Zhu, J.M., Johnson, D.H., Eastern Cooperative Oncology Group, 2002. N. Engl. J. Med. 346, 92-98.

Shtivelman, E., Hensing, T., Simon, G.R., Dennis, P.A., Otterson, G.A., Bueno, R., Salgia, R., 2014. Oncotarget 5, 1392-1433.

Shoja, Y., Rafati, A.A., Ghodsi, J., 2016a. Mater. Sci. Eng., C 58, 835-845.

Shoja, Y., Rafati, A.A., Ghodsi, J., 2016b, Electrochim. Acta 203, 281-291.

Song, Y., Li, Z., Guo, K., Shao, T., 2016. Nanoscale 8, 15671-15680.

Takata, M., Chikumi, H., Keiji Matsunami, K., Kodani,M., Sakamoto, T., Hashimoto, K., Nakamoto, M., Okada, K., Kitaura, T., Matsumoto, S., Kurai, J., Yamasaki, A., Igishi, T., Burioka, N., Shimizu, E., 2015. Oncol Rep. 3, 1040-1048.

Tan, Y.B., Lee, J.M., 2013. J. Mater. Chem. A 1, 14814-14843.

Tang, D.P., Yuan, R., Chai, Y.Q., 2008. Anal. Chem. 80, 1582-1588.

Tian, T., Liu, H., Li, L., Yu, J., Gea, S., Song, X., Yana, M., 2017. Sens. Actuators, B: chem 251, 440-445.

Topkaya, S.N., Azimzadeh, M., Ozsoz, M., 2016. Electroanalysis 28, 1-19.

Vellaisamy, K., Li, G., Ko, C.N., Zhong, H.J., Fatima, S., Kwan, H.Y., Wong, C.Y., Kwong, W.J., Tan, W., Leung, C.H., Ma, D.L., 2018. Chem. Sci. 9, 1119-1125.

Vinu, A., Hossian, K.Z., Srinivasu, P., Miyahara, M., Anandan, S., Gokulakrishnan, N., Mori, T., Ariga, K., Balasubramanian, V.V., 2007. J. Mater. Chem. 17, 1819-1825.

Wang, X.J., Yu, J.J., Sreekumar, A., Varambally, S., Shen, R., Giacherio, D., Mehra, R., Montie, J.E., Pienta, K.J., Sanda, M.G., Kantoff, P.W., Rubin, M.A., Wei, J.T., Ghosh, D., Chinnaiyan, A.M., 2005. New Engl. J. Med. 353, 1224-1235.

Wang, J., 2006a. Biosens. Bioelectron. 21, 1887-1892.

Wang, J., 2006b. Analytical Electrochemistry, 3rd edn. John Wiley and Sons. New York.

Wang, J., 2007. Electroanalysis 19, 769-776.

Wang, J., Cao, Y., Xu, Y.Y., Li, G.X., 2009a. Biosens. Bioelectron. 25, 532-536.

Wang, X., Dai, S., 2009b. Adsorption 15, 138-144.

Wang, L., Hua, E., Liang, M., Ma, C., Liu, Z., Sheng, S., Liu, M., Xie, G., Feng, W., 2014. Biosens. Bioelectron. 51, 201-207.

Wang, L., Guo, T., Lu, Q., Yan, X., zhong, D., Zhang, Z., Ni, Y., Han, Y., Cui, D., Li, X., Huang, L., 2015. ACS Appl. Mater. Interfaces. 7, 359-369.

Wang, M., Mao, Z., Kang, T.S., Wong, C.Y., Mergny, J.L., Leung, C.H., Ma, D.L., 2016. Chem. Sci. 7, 2516-2523.

Wu, X.Y., Liu, H.J., Liu, J.Q., Haley, K.N., Treadway, J.A., Larson, J.P., Ge, N.F., Peale, F., Bruchez, M.P., 2002. Nat. Biotechnol. 21, 41-46.

Xu, X.W., Weng, X.H., Wang, C.L., Lin, W.W., Liu, A.L., Chen, W., Lin, X.H., 2016. Biosens. Bioelectron. 80, 411-417.

Yang, W.C., Yu, M., Sun, X., Woolley, A.T., 2010. Lab Chip. 10, 2527-2533.

Ying, Z.M., Wu, Z., Tu, B., Tan, W., Jiang, J.H., 2017. J. Am. Chem. Soc. 139, 9779-9782.

Yong, K.T., Ding, H., Roy, I., Law, W.C., Bergey, E.J, Maitra, A., Prasad, P.N., 2009. ACS Nano. 3, 502-510.

Ziegler, A., Koch, A., Krockenberger, K., Großhennig, A., 2012. Hum. Genet. 131, 1627-1638.

Zhang, L.L., Zhou, R., Zhao, X.S., 2010. J. Mater. Chem. 20, 5983-5992.

Zhu, S.M., Zhou, H.S., Hibino, M., Honma, I., Ichihara, M., 2005. Adv. Funct. Mater. 15, 381-386.

Figure captions:

Scheme 1. Fabrication steps of the rGO/ssDNA-OMC/Ni NPs/PGE DNA electrochemical biosensor.

Figure 1. (a) XRD pattern of the Ni nanoparticles and (b) FE-SEM image of Ni nanoparticles electrodeposited on rGO/f-OMC/PGE.

Figure 2. (a) The chemical structure of the very possibly structure of the Ni‑OTC complex and (b) FE-SEM image of Ni-OTC nanoparticles

Figure 3. CVs of (a) bare PGE , (b) rGO/f-OMC/PGE, (c) rGO/f-OMC/Ni-OTC NPs/PGE and (d) rGO/ssDNA-OMC/Ni-OTC NPs/PGE in 0.1 M KCl solution containing 5.0 mM $K_3[Fe(CN)_6]$ at a scan rate of 100 mV/s.

Figure 4. The fitted I_{pa} (anodic peak current) versus the square root of the scan rates for CVs of rGO/f-OMC/Ni-OTC/PGE and rGO/ssDNA-OMC/Ni-OTC NPs/PGE in 0.1M KCl solution containing 5.0 mM $K_3[Fe\ (CN)_6]$.

Figure 5. (a) DPV voltammograms of rGO/f-OMC/Ni-OTC NPs/PGE (curve a), rGO/ssDNA-OMC/Ni-OTC NPs/PGE (curve b), after hybridization with DNA_C target (curve c) and after hybridization with sequences containing one-base mismatch target DNA_M (curve d) in NaOH 0.1 M, (b) responsibility of various electrodes. The error bar represents the standard deviation of threemeasurements.

Figure 6. Amperometric response of modified electrode in NaOH 0.1 M upon increasing the concentration of ssDNA target in the range of 0.1 µM to 3 µM under optimized condition.

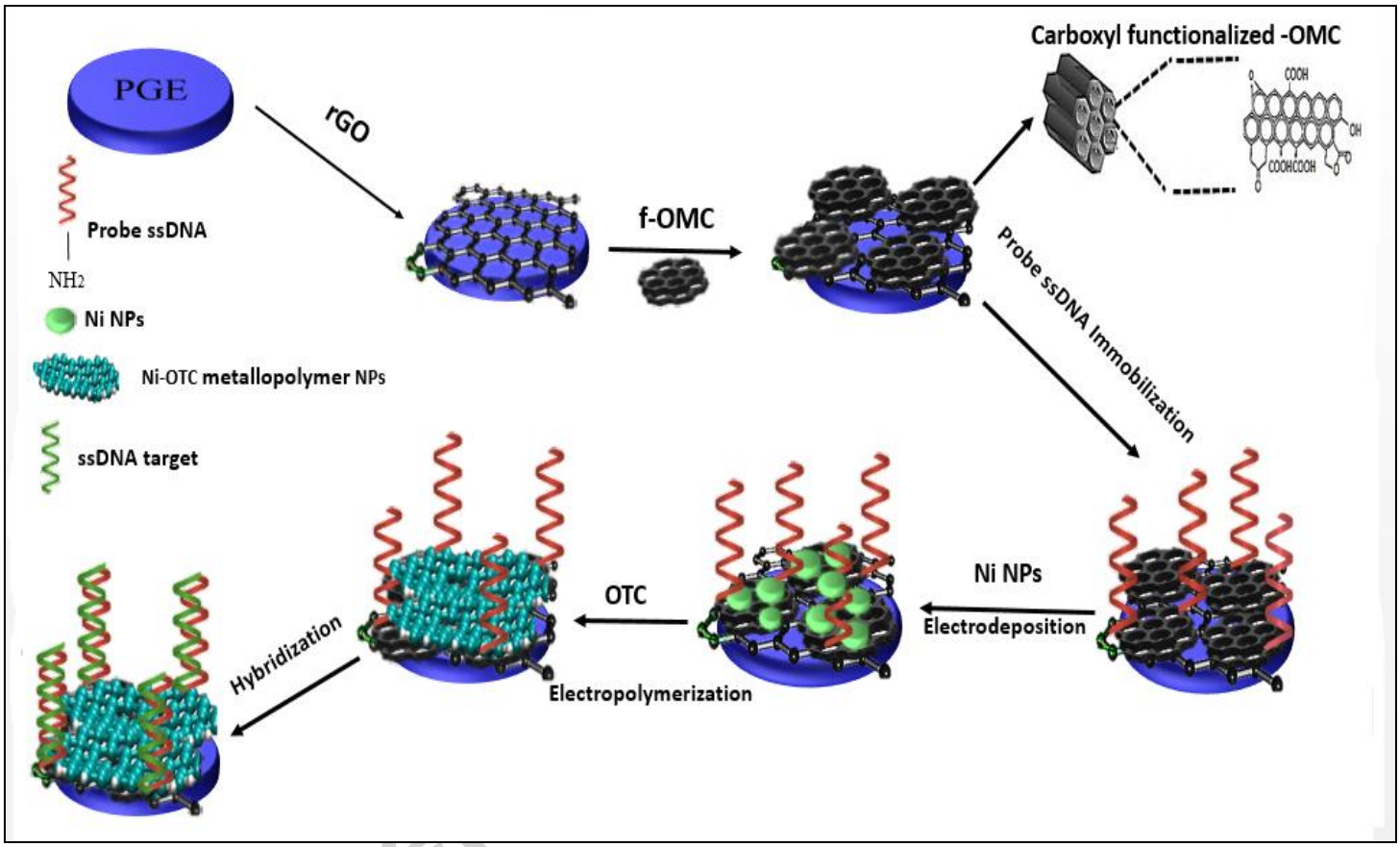
PGE
rGO
Carboxyl functionalized -OMC
COOH
OH
COOHCOOH
Probe ssDNA
NH2
f-OMC
Ni NPs
Ni-OTC metallopolymer NPs
ssDNA target
Probe ssDNA Immobilization
Ni NPs
Electrodeposition
OTC
Electropolymerization
Hybridization

Scheme 1.

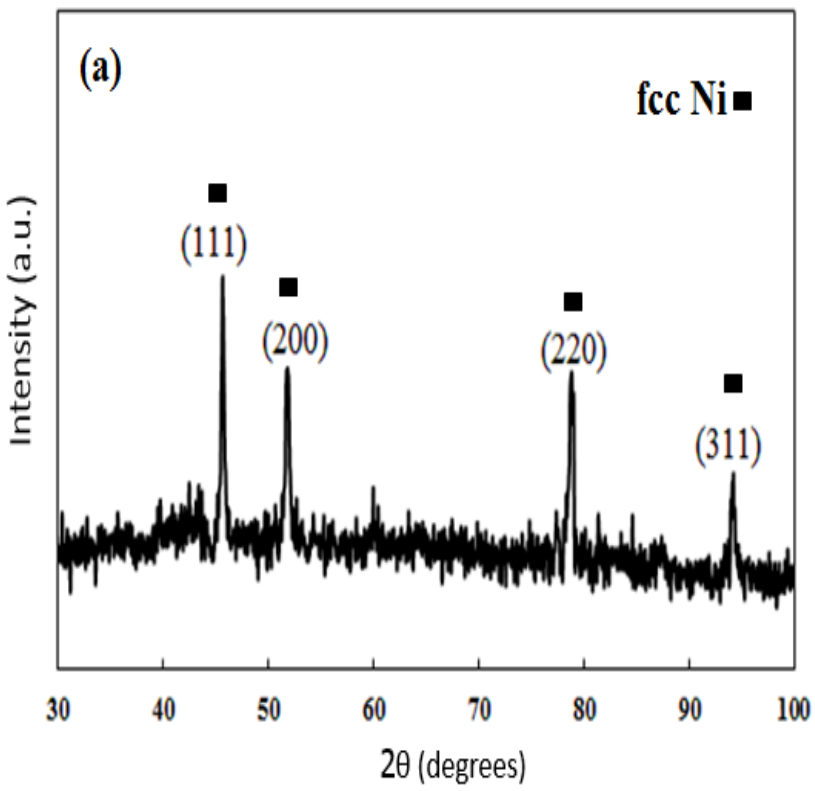
(a)
fcc Ni■
(111)
(200)
(220)
(311)
Intensity (a.u.)
30
40
50
60
70
80
90
100
2θ (degrees)

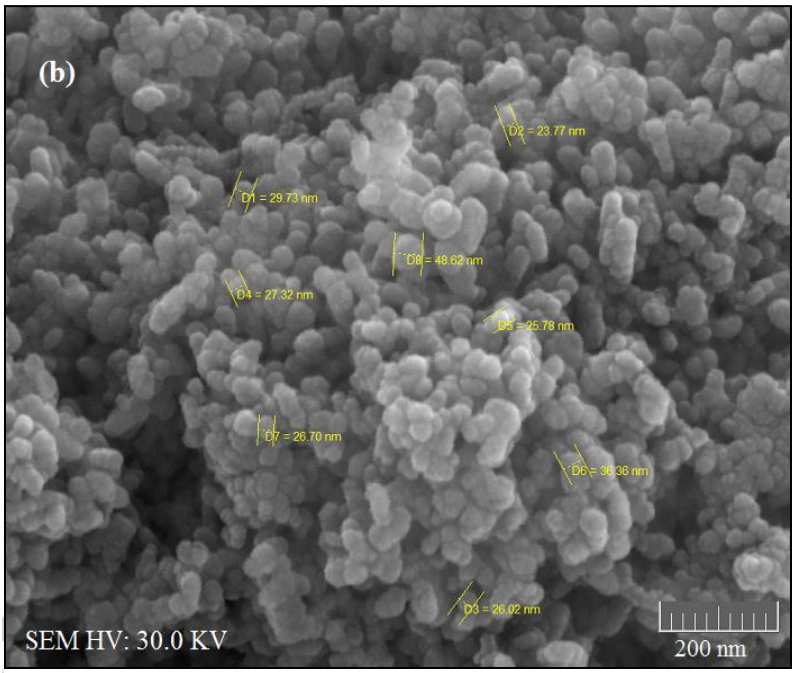
(b)
D2 = 23.77 nm
D1 = 29.73 nm
D8 = 48.62 nm
D4 = 27.32 nm
D5 = 25.78 nm
D7 = 26.70 nm
D6 = 30.36 nm
D3 = 26.02 nm
SEM HV: 30.0 KV
200 nm

Figure 1.

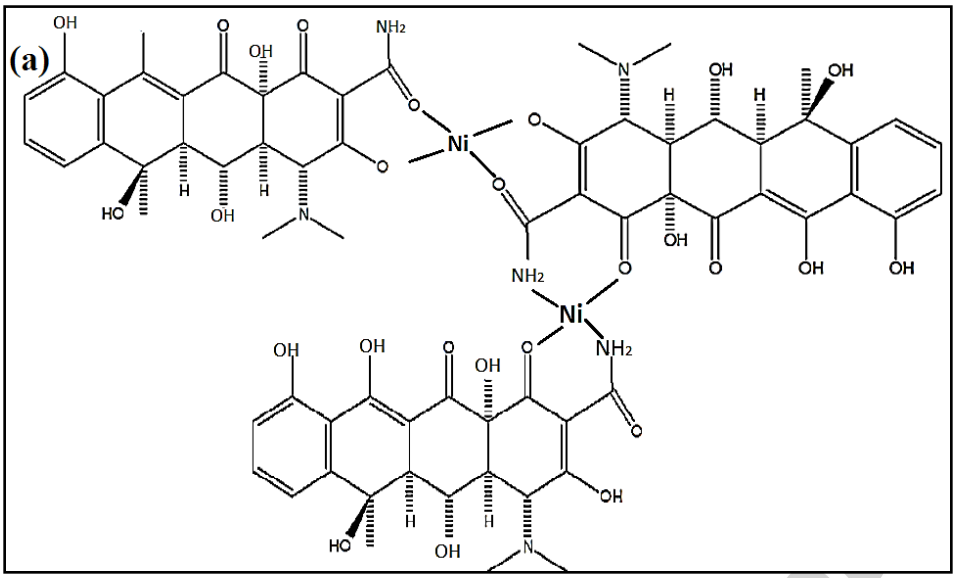
(a)
OH
O
NH2
Ni
N
H
HO
OH

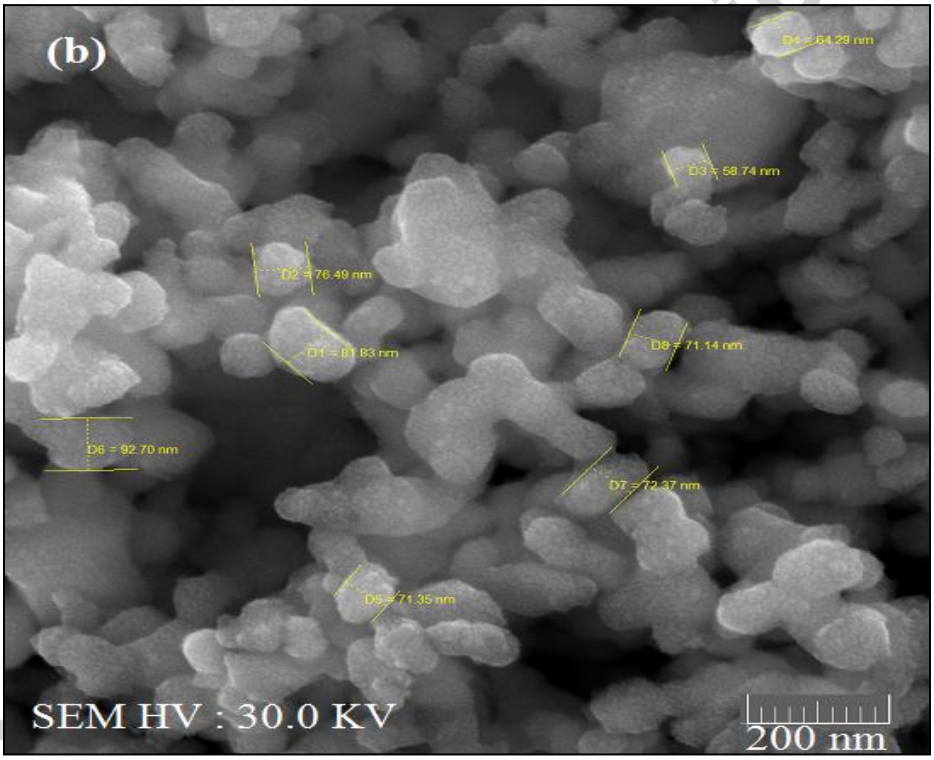
(b)
D4 = 64.29 nm
D3 = 58.74 nm
D2 = 76.49 nm
D1 = 81.83 nm
D8 = 71.14 nm
D6 = 92.70 nm
D7 = 72.37 nm
D5 = 71.35 nm
SEM HV : 30.0 KV
200 nm

Figure 2.

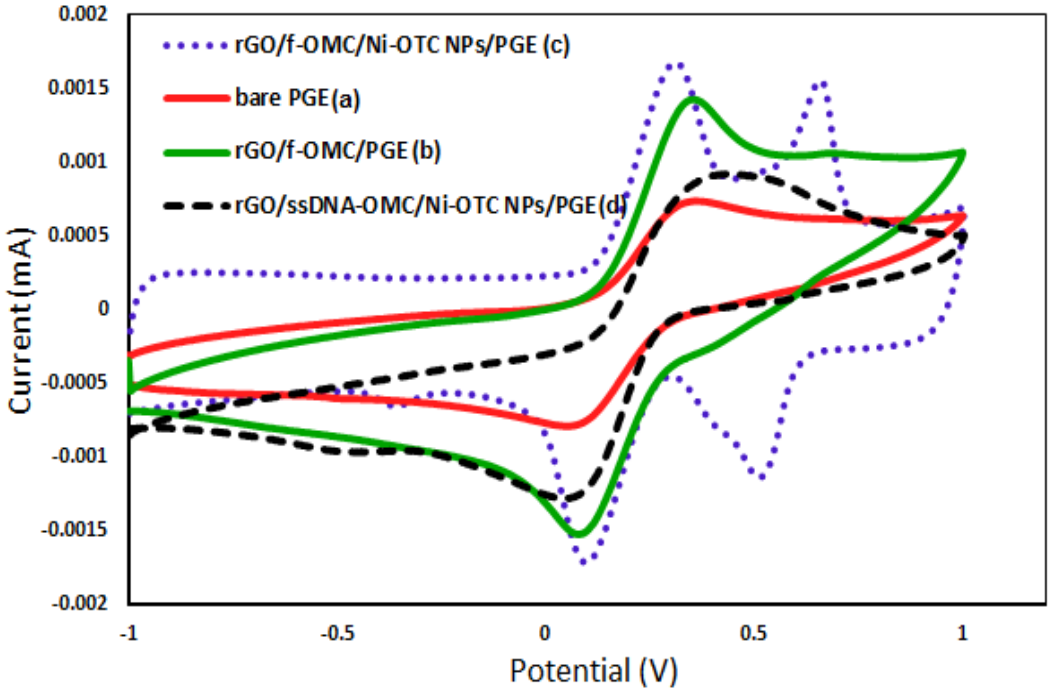
rGO/f-OMC/Ni-OTC NPs/PGE (c)
bare PGE (a)
rGO/f-OMC/PGE (b)
rGO/ssDNA-OMC/Ni-OTC NPs/PGE (d)
Current (mA)
Potential (V)
0.002
0.0015
0.001
0.0005
0
-0.0005
-0.001
-0.0015
-0.002
-1
-0.5
0
0.5
1

Figure 3.

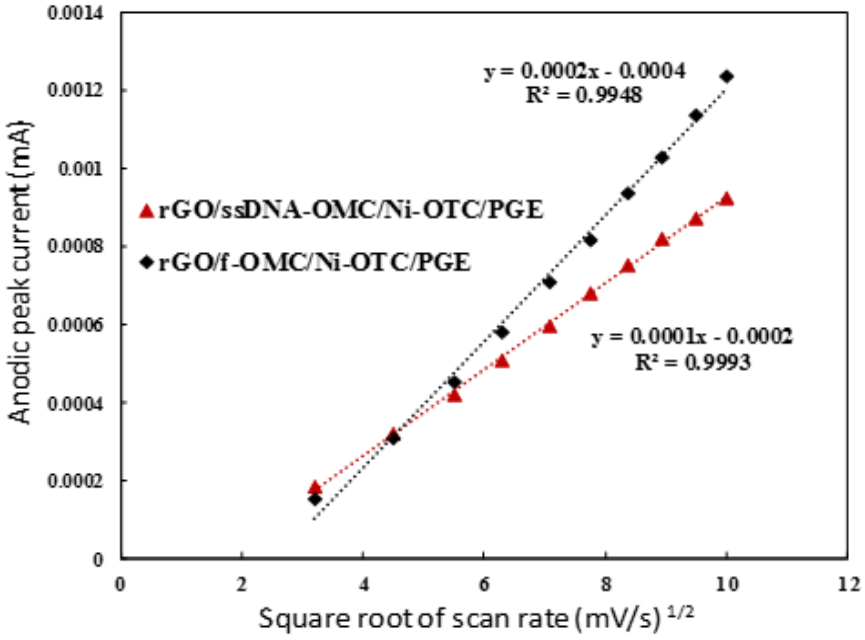

Figure 4.

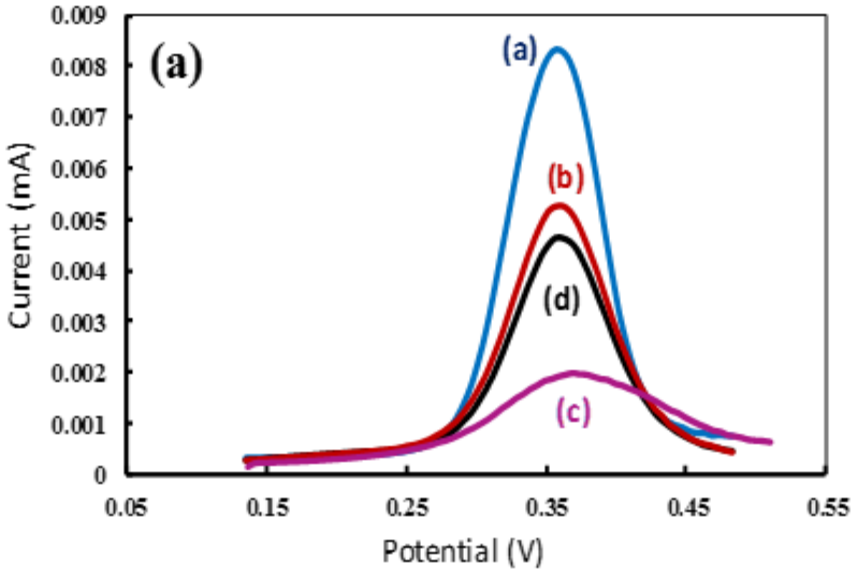
(a)
(a)
(b)
(d)
(c)
Current (mA)
Potential (V)
0.009
0.008
0.007
0.006
0.005
0.004
0.003
0.002
0.001
0
0.05
0.15
0.25
0.35
0.45
0.55

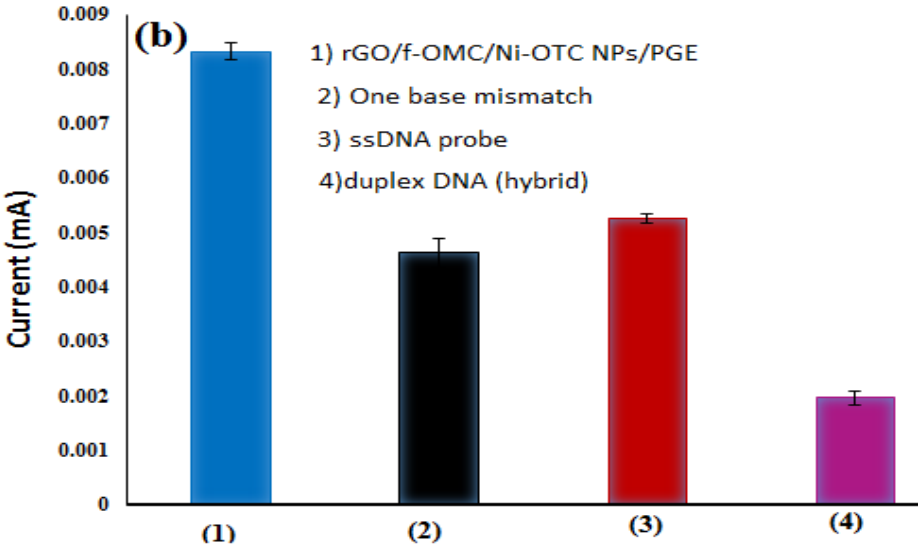
(b)
1) rGO/f-OMC/Ni-OTC NPs/PGE
2) One base mismatch
3) ssDNA probe
4)duplex DNA (hybrid)
Current (mA)
0.009
0.008
0.007
0.006
0.005
0.004
0.003
0.002
0.001
0
(1)
(2)
(3)
(4)

Figure 5.

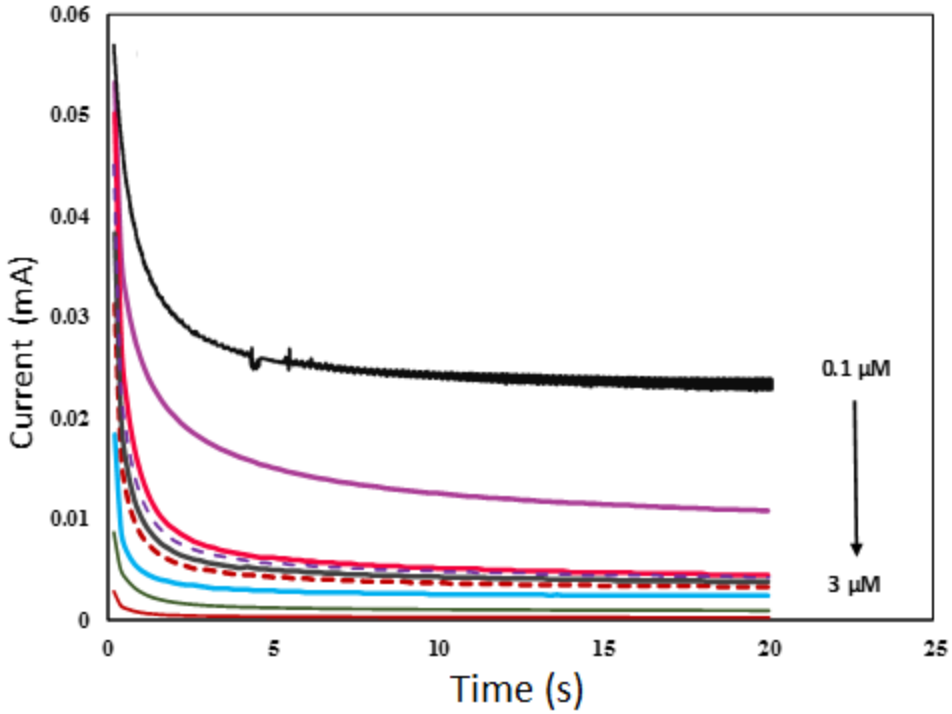

Figure 6.

Table 1. Comparison between of our developed DNA biosensor performance for detection EGFR exon21 mutation with some various methods previously reported.

Methods/Materials	Linear range (M)	Detection limit (nM)	Sensitivity	Reference
GSPE/PANI/Au NPs	2.0×10^{-10} to 1.0×10^{-8}	0.1	0.988 μA/nM	Saberi et al., 2013
N-G/Au NPs/GCE	1.0×10^{-14} to 1.0×10^{-7}	3.12×10^{-6}	26.91 μA/M	Chen et al., 2016
Au NPs/PANI/CS-GS/GCE	1.0×10^{-11} to 1.0×10^{-9}	2.11×10^{-3}	2.433 μA/pM	Wang et al., 2014
NiOx NPs/GCE	4.0×10^{-10} to 1.0×10^{-8}	6.8×10^{-2}	20.8 nA/nM	Noorbakhsha and Salimi., 2011
rGO/ss DNA-OMC/Ni-OTC NPs/PGE	1.0×10^{-7} to 3.0×10^{-6}	120	0.0188 mA/μM	This work

Highlights

- First report on EGFR exon 21 L858R mutation identification by novel DNA electrochemical biosensor.
- Modified ssDNA capture probe chemically immobilized at pencil graphite electrode modified with reduced graphene oxide /functionalized ordered mesoporous carbon/Ni-oxytetracycline metallopolymer nanoparticles in which Ni-oxytetracycline metallopolymer nanoparticles are as an electroactive label.
- Detection electrochemical signals exhibited linearity with complementary target DNA in the range of 0.1 μM to 3 μM under optimized condition.
- Characterization of developed electrochemical biosensor was done by FE-SEM, XRD, EDX, FT-IR, BET and CV. The response of proposed biosensor was investigated by differential pulse voltammetry and potentiostatic amperometry techniques
- The designed electrochemical biosensor showed good sensitivity, high reproducibility, repeatability, selectivity and stability.